Behavior of ductile short-grouted seismic reinforcing bar–to–foundation connections under adverse construction conditions

Theresa C. Aragon, Yahya C. Kurama, and Donald F. Meinheit

- This paper discusses the continuation of previous testing to aid in the development of a nonproprietary cementitious-grouted ductile connection to anchor energy-dissipating steel bars in gap-opening joints connecting precast concrete structures to foundations in seismic regions.
- Eight specimens were tested in an experimental program designed to investigate the effects of adverse construction conditions from excess water in the connection grout mixture and energy-dissipating bar offset in the connector sleeve.
- The research documented the ways that different grout products, bar embedment lengths, bar diameters, and connector sleeve taper angles affected the behavior of the connections and showed that reinforcing bars anchored over a short embedment length can achieve ductile cyclic behavior even under the adverse conditions that were considered.

PCI Journal (ISSN 0887-9672) V. 65, No. 4, July–August 2020.

PCI Journal is published bimonthly by the Precast/Prestressed Concrete Institute, 8770 W. Bryn Mawr Ave., Suite 1150, Chicago, IL 60631.

Ductile connections for anchoring energy-dissipating steel bars in gap-opening joints between the base of precast concrete structures and their foundations in seismic regions were tested by Aragon et al.[1,2] These tests were conducted in response to the need for a high-performing, simple, nonproprietary (that is, not requiring a specific grout product or proprietary connector), and low-cost system. Specifically, the connection is intended to allow ASTM A706[3] Grade 60 (414 MPa) deformed reinforcing bars that cross gap-opening joints between a precast concrete structure base (such as column, shear wall, and bridge pier bases) and the foundation to reach close to the full ultimate tensile strength and strain capacity of the reinforcing bar under cyclic loading.

The energy-dissipating bars in gap-opening precast concrete structures are critical to the behavior of the structure because they provide a significant portion of the lateral strength and most of the energy dissipation for the system during a large earthquake. Energy dissipation is achieved through yielding of the bars in tension during gap opening and yielding in compression during gap closing under the cyclic lateral displacements of the structure. A predetermined length of each reinforcing bar is prevented from bonding with the concrete by wrapping the bar inside a plastic sleeve at the gap-opening joint (above or below, or both) to significantly delay low-cycle fatigue fracture of the bar by distributing the steel strains nearly uniformly over the unbonded length. The unbonded length (also called the stretch length) is designed such that the maximum tension strains of the steel are

greater than $0.5\varepsilon_{uel}$ to provide adequate energy dissipation and smaller than $0.85\varepsilon_{uel}$ to prevent low-cycle fatigue fracture,[4] where ε_{uel} is the uniform elongation strain of the bar (that is, the strain at the maximum strength f_{uel}) measured from monotonic uniaxial tensile testing.[5]

Adequate development of the energy-dissipating bars inside the precast concrete element and the foundation is necessary for ductile behavior over large cyclic lateral displacements of the structure. The goal of the connections investigated by this research project is to anchor the bars over a short grouted embedment (bond) length rather than over the full required development length according to the American Concrete Institute's (ACI's) *Building Code Requirements for Structural Concrete (ACI-318-14) and Commentary (ACI 318R-14)*.[6] Bar embedment lengths shorter than the full ACI 318-14 development lengths are desirable because they reduce energy-dissipating bar lengths protruding out of the precast concrete base element and also reduce the amount of field grouting, thus simplifying the production, transportation, and erection of these structures. Research conducted by Smith et al.[5,7,8] for the validation of a hybrid precast concrete shear wall per ACI's *Acceptance Criteria for Special Unbonded Post-Tensioned Precast Structural Walls Based on Validation Testing and Commentary* (ACI ITG-5.1)[9] found that commercially available grouted Type II connectors cannot achieve adequate ductile energy-dissipating bar behavior at gap-opening joints. This finding led to the testing of the connections described in this paper.

In the following sections, a brief overview of the previous results from 12 specimens tested under ideal laboratory conditions (specimens 1 to 12) is presented first.[1,2] Then, the results from eight additional specimens (specimens 13 to 20) are described. Specimens 13 to 20 incorporate two adverse construction conditions that may be encountered in the field:

- The energy-dissipating bars were placed off-center with respect to the connector sleeve to simulate tolerance effects and misalignments.
- Excess water was used in the connection grout to simulate potential grout mixing errors resulting in grout strengths lower than the specified strength.

More information on the grouted reinforcing bar connections can be found in Aragon.[10]

Previous work

Figure 1 shows the setup that was used to test specimens 1 to 12.[1,2] The following findings were made based on the results of the following tests:

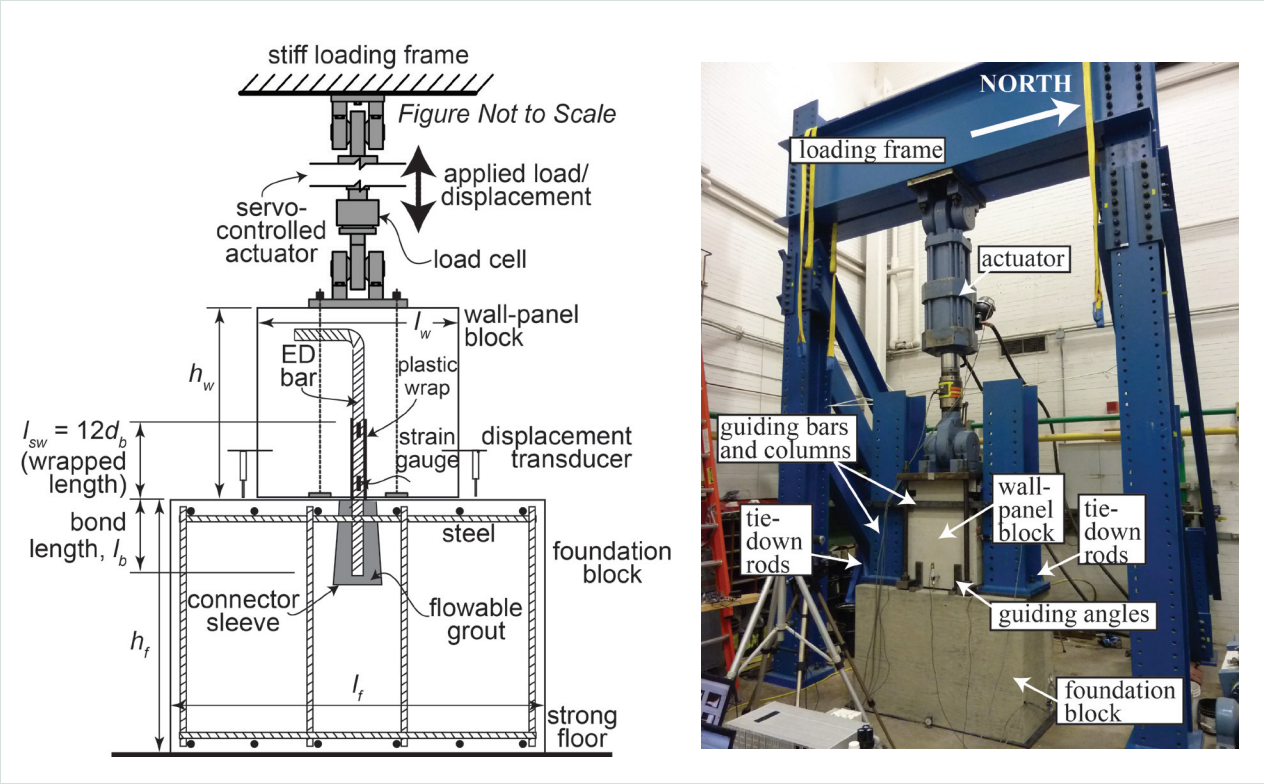

Figure 1. Energy-dissipating bar connection test setup. Note: Figure is not drawn to scale. d_b = nominal diameter of energy-dissipating bar; ED = energy-dissipating; h_f = height of foundation block; h_w = height of wall-panel block; l_b = embedment (bond) length of energy-dissipating bar; l_f = length of foundation block; l_{sw} = wrapped length of energy-dissipating bar; l_w = length of wall-panel block.

- A bond (embedment) length l_b equal to $10d_b$, where 10 is the bond length factor and d_b is the nominal bar diameter, was adequate to reach large cyclic energy-dissipating bar strains for no. 7 (22M) energy-dissipating bars (specimens 1 to 6). However, no. 9 and 11 (29M and 36M) bars (specimens 11 and 12, respectively) caused more demanding conditions on the connector grout, resulting in reduced cyclic strain capacities due to bar pullout despite the proportionally increased bond length with the bar diameter d_b (that is, $l_b = 10d_b$). Therefore, the optimal bond length factor may depend on the bar diameter. In other words, the bond length factor may need to be increased for larger bar diameters to achieve ductile behavior of the connection.

- The tested connector sleeve with a taper angle θ_d of 9.0 degrees (specimen 4) resulted in less grout bulging from the top of the sleeve during tension loading of the bar than sleeves with a 4.5-degree taper angle, but the tested sleeves with a 4.5-degree taper angle were deemed more practical while still providing the desired connection performance for no. 7 (22M) energy-dissipating bars. Further investigations are needed on connector sleeves with taper angles less than 4.5 degrees.

- Large variations were measured in the monotonic uniform elongation strain ε_{uel} and fracture strain $\varepsilon_{s,fr}$ of ASTM A706[3] bars from different manufacturing heats and of different sizes. There were also large variations in the low-cycle fatigue fracture strains of the energy-dissipating bars under cyclic loading, with some of the bars (specimens 7 and 9) fracturing at particularly low tension strains. Therefore, careful consideration should be taken to acquire reinforcing bars with large ε_{uel} and $\varepsilon_{s,fr}$ for use across gap-opening joints in precast concrete structures.

- Three different commercially available high-performance grout products (GM1, GM2, and GM3) were investigated. In general, connections with grout products GM1 and GM2 performed considerably better under cyclic loading than connections with grout product GM3. Connections with GM3 were more susceptible to bond failure (pullout) of the energy-dissipating bar inside the connector sleeve. A subsequent grout study involving monotonic bond pullout tests and modulus of rupture tests, and microscopic characterization showed relatively small differences among the grout products, and was not conclusive in identifying the cause of the significantly inferior performance of GM3 during the cyclic connection tests. Because the objective of this research is to develop a system that does not require a specific grout product, the bond length of the energy-dissipating bars may need to be increased to prevent bond failure, independent of the grout product used.

Experimental program

Based on the results from specimens 1 to 12, three primary objectives were developed for the next phase of testing—specimens 13 to 20—described in this paper.

- objective 1: to determine whether a slightly increased energy-dissipating bar bond length factor can provide ductile performance of the connection under adverse conditions of energy-dissipating bar offset within the sleeve and reduced grout strength (simulated by using excess mix water), especially using grout product GM3, which showed poor performance in the previous tests

- objective 2: to investigate the effect of the energy-dissipating bar diameter d_b on the connection performance

- objective 3: to investigate the effect of the sleeve taper angle θ_d on the connection performance

The same test setup from Aragon et al.[1,2] (Fig. 1) was used in the tests. Each specimen consisted of a wall-panel block and a foundation block that were constructed separately and then connected using a single energy-dissipating bar. The foundation block was fixed to the laboratory strong floor during testing, and the wall-panel block was moved vertically using a 220 kip (979 kN) servo-controlled hydraulic actuator to subject the energy-dissipating bar to a rigorous quasi-static cyclic uniaxial strain history.[1,2] The actual applied strain history varied slightly among the tests but was consistent with the recommended loading for the validation of energy-dissipating bar connections in gap-opening joints of seismic precast concrete walls.[1,2,5] To allow the energy-dissipation bar to be loaded into a small amount of compression strain (after each tension loading excursion) without the wall-panel block coming into full contact with the foundation block, a small initial gap was created using 0.015 in. (0.38 mm) thick temporary steel shims that were removed prior to testing at the horizontal joint between the two blocks. Note that in practice, the joint between the base of a precast concrete member and the foundation would normally be filled with grout (approximately 0.5 to 1.0 in. [13 to 25 mm] thick) for tolerance and erection alignment purposes. Because the presence of this grout pad was not expected to affect the performance of the energy-dissipation bar connection, the joint between the wall-panel and foundation blocks in this experimental program was not grouted (for ease of construction).

The grouted connector sleeve was centered at the top of the foundation block; however, unlike the previous tests for specimens 1 to 12, the energy-dissipating bar was placed axially off-center within the connector sleeve to simulate an adverse situation that may occur in the field. All specimens used ASTM A706[3] Grade 60 (414 MPa) energy-dissipating bars with the following bar sizes:

- Specimens 13 and 14 used no. 7 (22M) reinforcing bars (nominal diameter d_b = 0.875 in. [22.2 mm]).

- Specimen 15 used no. 9 (29M) reinforcing bars (d_b = 1.128 in. [28.7 mm]).

- Specimens 16 to 20 used no. 11 (36M) reinforcing bars (d_b = 1.410 in. [35.8 mm]).

As described in Aragon et al.,[1,2] each energy-dissipating bar was unbonded from the concrete by wrapping it inside a plastic sheeting over a length of $l_{sw} = 12d_b$ at the bottom of the wall-panel block. **Table 1** shows the connector sleeve and energy-dissipating bar properties for specimens 13 to 20. Similar information for specimens 1 to 12 can be found in Aragon et al.[1,2]

Each wall-panel block was designed to represent a portion of the length of a precast concrete wall panel at the base and was reinforced with nominal no. 3 (10M) deformed ASTM A615 Grade 60 (414 MPa)[11] bars similar to the reinforcement of the wall-panel blocks described in Aragon et al.[1,2] Each wall panel had a thickness (width) t_w of 15 in. (380 mm) and length l_w of 24 in. (610 mm). The height of the wall-panel block h_w was controlled by the hooked energy-dissipating bar development length at the top end of the bar, based on section 25.4.3 of ACI 318-14.[6] The wall panels that used no. 7 (22M) energy-dissipating bars with a 90-degree hook (specimens 13 and 14) had a height h_w of 32 in. (810 mm). Specimens 15 to 20, which used no. 9 and 11 (29M and 36M) energy-dissipating bars with a 180-degree hook, had a wall-panel height h_w of 48 in. (1220 mm). In practice, hooked ends would not be needed to achieve full development at the top of the energy-dissipating bars because the height of a full-size wall panel would allow full development using a straight bar.

The foundation block for specimens 13 to 20 had a width w_f of 24 in. (610 mm) and a length l_f of 54 in. (1370 mm). The height of the foundation block h_f was controlled by the grouted connector bond lengths of the energy-dissipating bars. Each foundation block was designed to be reused in two tests and accommodate two energy-dissipating bar connector sleeves (one on top and one on the bottom of the block) by rotating the top of the block with respect to the bottom after the completion of a test. The foundation block for specimens 13 and 14 with no. 7 (22M) energy-dissipating bars had a height h_f of 36 in. (910 mm), and for specimens 15 through 20 with no. 9 and 11 (29M and 36M) energy-dissipating bars, h_f was equal to 49 in. (1245 mm). The same strut-and-tie analysis procedure that was used to prevent breakout of the concrete surrounding the energy-dissipating bar connections in specimens 1 to 12[1,2] was followed in the design of the vertical and horizontal tie reinforcement placed around each connector sleeve inside the foundation block of specimens 13 to 20. Details of this strut-and-tie model and the ASTM A615 Grade 60 (414 MPa) tie reinforcement used in the foundation block for the different energy-dissipating bar sizes can be found in Aragon[10] and Aragon et al.[1,2]

Figure 2 shows photographs and outer dimensions of the connector sleeves used in specimens 13 to 20, and **Tables** 1 and **2** list their properties. All of the connector sleeves were made by a local sheet metal manufacturer using 25-gauge nongalvanized smooth sheet steel with a measured thickness of 0.0209 in. (0.531 mm), with or without added corrugations, except for the connector in specimen 20, which was a commercially available corrugated steel pipe typically used in the post-tensioning industry. For practical tolerance purposes, the connector sleeves were slightly longer than the embedment bond length of the energy-dissipating bars, and the diameter of each sleeve was oversized to provide adequate clearance and tolerance for the placement of the energy-dissipating bar.

Simulated adverse field conditions

All grout products used in this research satisfied ASTM C1107[12] for prepackaged, nonshrink, dry, hydraulic-cement grout. A 50 lb (23 kg) bag of grout was mixed for each connection; however, to simulate potential adverse conditions that may occur in the field, an excess amount of water (in addition to the manufacturer's specifications for a

Table 1. Connector properties

Specimen	Connector sleeve					Energy-dissipating bar		
	Taper angle θ_d, degrees	Entrance diameter, in.	Bottom diameter, in.	Surface corrugations	Length, in.	Size, no.	Wrapped length l_{sw}, in.	Bond length l_b, in.
13	4.5	2.75	4.50	Manually placed	12.5	7	10.5 ($12d_b$)	10.5 ($12d_b$)
14	4.5	2.75	4.50	Manually placed	12.5	7	10.5 ($12d_b$)	10.5 ($12d_b$)
15	4.5	3.00	5.50	None	15.5	9	13.5 ($12d_b$)	13.5 ($12d_b$)
16	4.5	3.25	6.25	None	19.0	11	16.9 ($12d_b$)	16.9 ($12d_b$)
17	1.5	3.25	4.50	None	23.0	11	16.9 ($12d_b$)	21.2 ($15d_b$)
18	3.0	3.25	5.63	None	23.0	11	16.9 ($12d_b$)	21.2 ($15d_b$)
19	4.5	3.25	6.88	None	23.0	11	16.9 ($12d_b$)	21.2 ($15d_b$)
20	0.0	3.25	3.25	Automated	23.0	11	16.9 ($12d_b$)	21.2 ($15d_b$)

Note: d_b = nominal diameter of energy-dissipating bar. No. 7 = 22M; no. 9 = 29M; no. 11 = 36M; 1 in. = 25.4 mm.

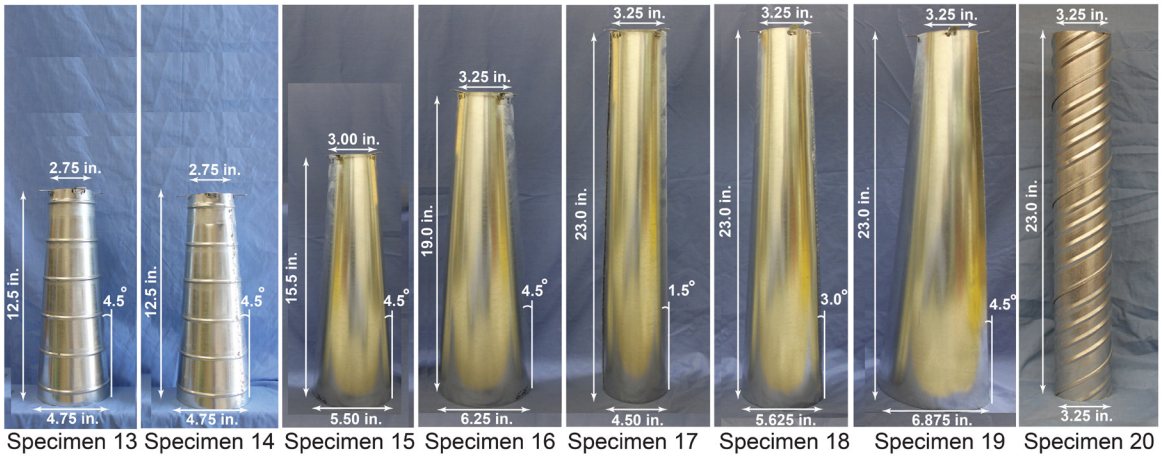

Figure 2. Connector sleeves. Note: 1 in. = 25.4 mm.

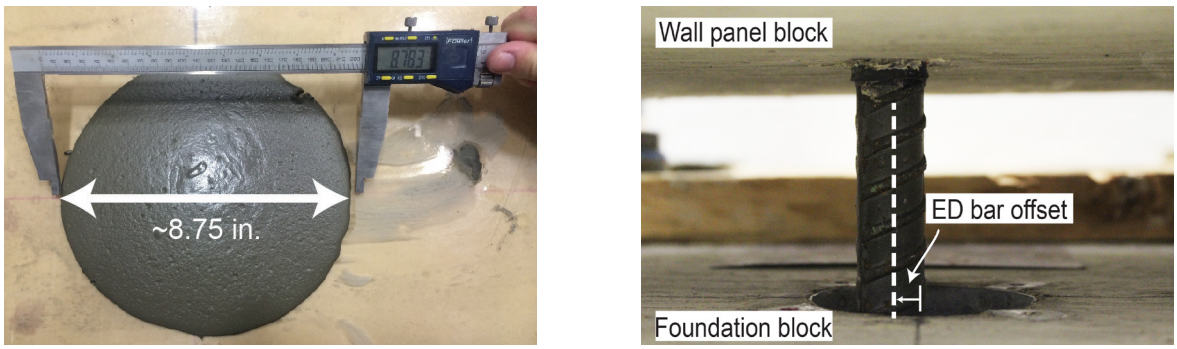

Figure 3. Adverse conditions of increased water in grout (increased flow diameter) and energy-dissipating (ED) bar axial offset.

Table 2. Grout properties

Specimen	Grout product	Target 28-day compressive strength, psi	Flow diameter, in.	Average 28-day compressive strength $f'_{cg,28d}$, psi	Average connection test-day compressive strength f'_{cg}, psi	Connection test-day age, days
13	GM2	<8000	8.78	7326	7350	39
14	GM3	<8000	8.75	7174	7400	44
15	GM3	<8000	8.50	7298	7386	36
16	GM3	<8000	8.38	7161	7203	32
17	GM3	<8000	8.44	7590	7692	32
18	GM3	<8000	8.69	7099	7181	31
19	GM3	<8000	8.81	7252	7421	29
20	GM3	<8000	8.69	7452	7580	43

Note: 1 in. = 25.4 mm; 1 psi = 6.895 kPa.

flowable grout consistency) was intentionally added to each batch with the goal of achieving grout compressive strengths lower than f'_{cg} = 8000 psi (55.2 MPa). Grout product GM2 was used for specimen 13 and GM3 was used for specimens 14 to 20. Immediately after mixing, the flow diameter (spread) of the grout was measured using a 2 in. (50 mm) diameter × 4 in. (100 mm) tall plastic cylinder that was filled with grout and slowly lifted on top of a flow template. The target spread diameter in specimens 1 to 12, except for specimen 10, was 5 to 6 in. (125 to 150 mm), resulting in average grout compressive strengths f'_{cg} varying between 8310 and 10,324 psi (57.3 and 71.2 MPa).[1,2] With the excess water added to the grout mixtures for specimens 13 to 20, the spread diameter varied between 8.38 and 8.81 in. (213 and 224 mm) (**Fig. 3**), resulting in average 28-day grout compressive strengths $f'_{cg,28d}$ ranging between 7099 and 7590 psi (48.9 and 52.3 MPa).

In addition to the grout mixture water adjustments, the energy-dissipating bar in each specimen was placed with a clear distance of approximately 0.25 in. (6.4 mm) from the inner edge of the entrance (top) diameter of the connection sleeve, resulting in an axial offset from the center of the sleeve (Fig. 3), while still maintaining vertical alignment of the bar with the centerline of the sleeve (that is, the bar was placed parallel to the centerline of the sleeve but with an axial offset).

Specimens 13 and 14: Objective 1

Specimens 13 and 14 (using grout products GM2 and GM3, respectively) specifically targeted objective 1 by testing no. 7 (22M) energy-dissipating bars with a slightly longer embedment length l_b equal to $12d_b$ (instead of $10d_b$ in the previous specimens[1,2]) to determine whether this increase in the bond length factor can result in ductile connection performance under the adverse conditions of energy-dissipating bar offset within the connection sleeve and increased water in the grout. The energy-dissipating bar offset was 0.69 in. (17.5 mm) from the center of the sleeve. The connection sleeves had the same dimensions: top diameter = 2.75 in. (69.9 mm), length = 12.5 in. (317 mm), and taper angle θ_d = 4.5 degrees. In addition, the sleeves had surface corrugations (deformations) that were placed manually in a circumferential pattern during the manufacturing of the sleeves. The corrugations were spaced at approximately 2.0 in. (50 mm) and had a depth d_{corr} of 0.0625 in. (1.59 mm).

Specimens 15 and 16: Objective 2

Specimens 15 and 16 specifically targeted objective 2 by testing whether an increased bond length factor of 12 (l_b = $12d_b$) can achieve ductile connector performance using grout product GM3 with no. 9 and 11 (29M and 36M) energy-dissipating bars, respectively. The connector sleeves had smooth (uncorrugated) surfaces and a 4.5-degree taper. For tolerance purposes like in the other specimens, the sleeves were fabricated to be slightly longer (15.5 and 19.0 in. [394 and 483 mm]) than the embedment length of the no. 9 and 11 energy-dissipating bars, respectively. In addition, the bar entry diameter (sleeve top diameter) was oversized to 3.0 in. (75 mm) for the no. 9 energy-dissipating bar and 3.25 in. (82.6 mm) for the no. 11 energy-dissipating bar. Similar to specimens 13 and 14, each connection was tested under adverse conditions with increased water in the grout and energy-dissipating bar offset within the tapered sleeve. The bar offset was 0.69 and 0.67 in. (17.4 and 17.0 mm) from the center of the sleeve for the no. 9 and 11 energy-dissipating bars, respectively.

Specimens 17 to 20: Objective 3

Specimens 17 to 20 targeted objective 3 by testing the effect of the sleeve taper angle (θ_d equal to 1.5, 3.0, 4.5, and 0.0 degrees, respectively) on the connector performance, all using no. 11 (36M) energy-dissipating bars, which was the largest bar size tested in the experimental program. These specimens were also constructed with increased water in the grout (GM3) and energy-dissipating bar offset within the sleeve. The concrete wall-panel and foundation blocks for specimens 15 through 20 were all constructed on the same day using the same delivery of ready-mixed concrete, rather than in groups of casting. Because of this, there was a concern that if all of these specimens were made to accommodate a bond length l_b equal to $12d_b$ and if it was determined after testing specimen 16 that the $12d_b$ bond length was not long enough to achieve ductile failure, then the remaining specimens (specimens 17 to 20) would also fail prematurely. Therefore, the energy-dissipating bars within the wall panels for specimens 17 to 20 were constructed with a protruding length of $15d_b$, and the connector sleeve length in the corresponding foundation blocks for these specimens was adequate for a $15d_b$ bond length. This allowed for a bond length of up to $15d_b$ to be used in specimens 17 to 20. If specimen 16 exhibited ductile performance, then the protruding (bond) bar length for the remaining specimens could be reduced by saw cutting the end of the energy-dissipating bar before grouting it into the connector sleeve. As such, the test results from specimens 17 to 20 could also contribute to objective 2.

As shown in Fig. 2 and listed in Table 1, the top (entry) diameter of the connector sleeves for specimens 17 to 20 was the same (3.25 in. [82.6 mm]) as that for specimen 16, but the length of the sleeves was increased to 23.0 in. (584 mm) to accommodate the potentially greater bond length of $15d_b$ in specimens 17 to 20. Specimens 17 to 19 did not have corrugations on the surface of the connector sleeves. The straight sleeve in specimen 20 was a commercially available corrugated steel pipe, typically used in the post-tensioning industry, made of 25-gauge ASTM A653[13] galvanized strip steel material with a measured thickness of 0.0217 in. (0.551 mm). In the previous tests described in Aragon et al.,[2] specimen 9 also used a commercially available straight steel pipe typically used in the post-tensioning industry, but from a different pipe manufacturer than the sleeve in specimen 20. The depth of the sleeve corrugations d_{corr} (0.0625 in. [1.59 mm]) in specimen 20 was smaller than that in specimen 9 (d_{corr} = 0.1875 in. [4.76 mm]), but was similar to the other sleeves with corrugations in specimens 2,

3, 4, 6, 13, and 14 (tapered sleeves) and specimen 5 (straight sleeve), which had corrugations placed manually during the manufacturing of the sleeves from smooth sheet steel. Furthermore, the sleeve corrugations in specimen 20 were spaced farther apart, at 1.0 in. (25 mm) spacing, than the specimen 9 sleeve corrugations, which were spaced at 0.65 in. (16.5 mm). The sleeve corrugations in both specimens 20 and 9 had a continuous helical (spiral) pattern (unlike the sleeves in all other specimens with manually placed individual circumferential corrugations, including specimen 5 with a straight sleeve connector). In addition, there was a distributed dimple pattern on the inside surface of the sleeve in specimen 20 (unlike the sleeves in all of the other specimens, including specimens 5 and 9 with straight sleeve connectors), thus increasing the inside surface roughness. Full details and comparisons of the surface corrugation patterns and dimensions on all of the connection sleeves can be found in Aragon.[10]

Energy-dissipating bar stress-strain properties

The monotonic tension stress-strain behavior of the ASTM A706 Grade 60 (414 MPa) energy-dissipating reinforcement was determined by testing three samples for each bar in a hydraulic universal testing machine. The bar strains in these material tests were measured using an extensometer with a 2 in. (50 mm) gauge length placed over the free length of the bar between the wedge grips of the testing machine. The extensometer was removed before bar fracture, to prevent damage to the sensor, but after the bar had reached the maximum stress f_{uel} and corresponding uniform elongation strain ε_{uel} and had undergone an approximately 0.5% decrease in stress from f_{uel}. The subsequent incremental strains (that is, additional strains after removal of the extensometer) were calculated approximately using the relative displacements of the testing machine crossheads.

Large variations were observed in both the uniform elongation strain ε_{uel} and fracture strain $\varepsilon_{s,fr}$ of the ASTM A706 reinforcing bars from the different heats and for the different bar sizes used in Aragon et al.[1,2] Specifically, the maximum deformation capacity of the connection can be limited by premature low-cycle fatigue fracture of the energy-dissipating bar. Therefore, careful consideration was taken to acquire bars with large fracture strain $\varepsilon_{s,fr}$ values (provided on the manufacturer mill certifications) for use in specimens 13 to 20.

The no. 7 (22M) energy-dissipating bars in specimens 13 and 14 were from a single manufacturing heat (called no. 7–heat 3 herein) but were provided by a different manufacturer than the no. 7 bars in specimens 1 to 6 and 7 to 10 (no. 7–heat 1 and no. 7–heat 2, respectively). **Figure 4** shows the typical measured monotonic tension stress-strain behavior of a single bar tested for each of the three heats of no. 7 bars, where it can be seen that the uniform elongation strain ε_{uel} and fracture strain $\varepsilon_{s,fr}$ of the no. 7–heat 3 bars were smaller than those for the no. 7–heat 1 bars but greater than those for the no. 7–heat 2 bars.

Similarly, the no. 9 (29M) energy-dissipating bar in specimen 15 (no. 9–heat 2) was provided by a different manufacturer than the no. 9 bar in specimen 11 (no. 9–heat 1). Figure 4 shows that the no. 9–heat 2 energy-dissipating bars had larger ε_{uel} and $\varepsilon_{s,fr}$ than the no. 9–heat 1 bars.

The no. 11 (36M) bars in specimens 16 to 20 were also from a single manufacturing heat (no. 11–heat 2) and again were

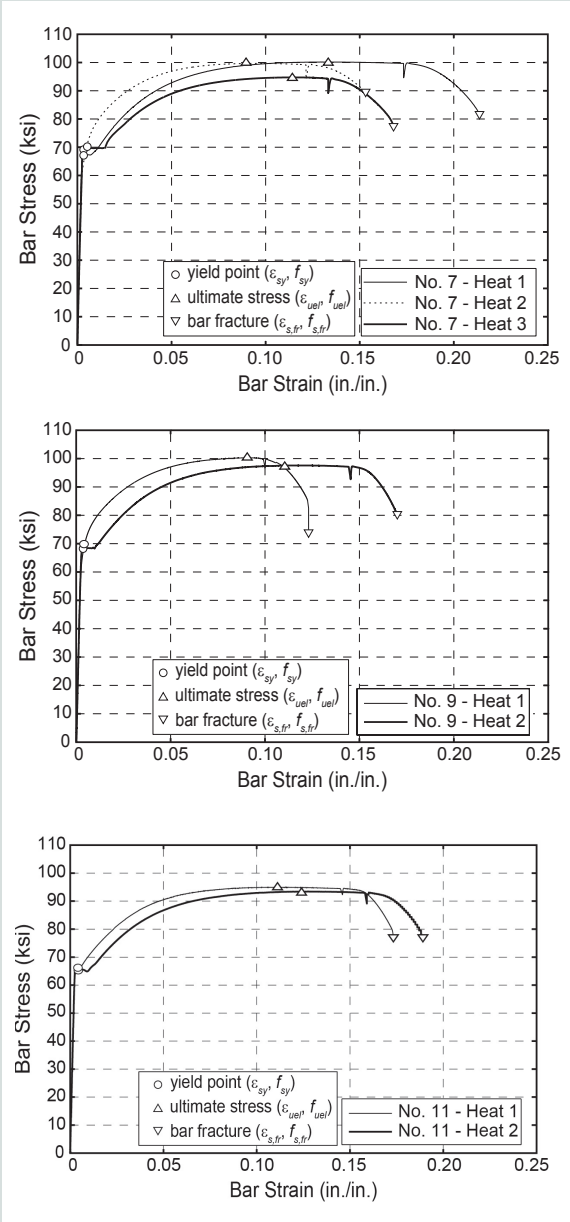

Figure 4. No. 7, no. 9, and no. 11 energy-dissipating bar stress-strain behaviors under monotonic tension loading. Note: $f_{s,fr}$ = stress in energy-dissipating bar at fracture; f_{sy} = yield strength of energy-dissipating bar; f_{uel} = ultimate (maximum) strength of energy-dissipating bar; $\varepsilon_{s,fr}$ = strain in energy-dissipating bar at fracture; ε_{sy} = yield strain of energy-dissipating bar; ε_{uel} = uniform elongation strain of energy-dissipating bar at f_{uel}. No. 7 = 22M; no. 9 = 29M; no. 11 = 36M; 1 in. = 25.4 mm; 1 ksi = 6.895 MPa.

provided by a different manufacturer than the no. 11 bar in specimen 12 (no. 11–heat 1). The no. 11–heat 2 bars had larger ε_{uel} and $\varepsilon_{s,fr}$ than the no. 11–heat 1 bars (Fig. 4).

Table 3 lists the important mechanical properties for the energy-dissipating bars in specimens 13 to 20. Similar information for the bars in specimens 1 to 12 (no. 7–heat 1, no. 7–heat 2, no. 9–heat 1, and no. 11–heat 1) can be found in Aragon et al.[1,2] The yield strength f_{sy} and yield strain ε_{sy} were determined at the initiation of the yield plateau. The modulus of elasticity (Young's modulus) E_s was calculated as the ratio of the difference between two stresses (20 and 50 ksi [138 and 345 MPa]) within the initial linear-elastic range and the difference between the two corresponding strains. The uniform elongation strain ε_{uel} was determined at the maximum (peak) strength f_{uel} of the measured stress-strain behavior. Based on the material testing, all of the energy-dissipating bars satisfied all requirements for ASTM A706 steel, including the minimum elongation requirement (that is, fracture strain $\varepsilon_{s,fr}$) of 12% for Grade 60 (414 MPa) no. 7, 9, and 11 reinforcing bars.

Figure 4 and the values listed in Table 3 highlight the large variations in the uniform elongation strain ε_{uel} and fracture strain $\varepsilon_{s,fr}$ of the ASTM A706 bars from the different heats and for the different bar sizes. Importantly, ACI ITG-5.2[4] specifies a maximum allowable energy-dissipating bar tension strain of $0.85\varepsilon_{uel}$ for use in the design of gap-opening precast concrete joints for seismic regions. However, because values of ε_{uel} for ASTM A706 bars can vary greatly, validation of ductile energy-dissipating bar connections based on the achievement of a prescribed maximum tension strain value rather than strain as a proportion of ε_{uel} would result in more consistent performance requirements. Therefore, for the study described in this paper, a constant target maximum energy-dissipating bar strain of 0.06 in./in. (0.06 mm/mm) was deemed appropriate for the cyclic load validation of the ductile connections. This target strain capacity was selected based on the maximum energy-dissipating bar strains from the precast concrete shear wall specimens tested according to ACI ITG-5.1[9] in Smith et al.[5] and the full-scale wall design example in Smith and Kurama,[7] as well as the precast walls analyzed in Kurama.[14]

Connection test results

Figure 5 shows the measured cyclic energy-dissipating bar strain plotted against bar stress from testing of the connections in specimens 13 to 20. The measured monotonic tension strain versus stress behaviors from the corresponding three energy-dissipating bar material test samples are also included in each graph. To determine the energy-dissipating bar strains from the connection tests, the average relative displacement (that is, the joint separation measured by four linear variable displacement transducers [LVDTs]) between the wall-panel and foundation blocks was divided by the total estimated unbonded length l_{su} of $13d_b$ (that is, $12d_b$ of wrapped length plus an assumed $1d_b$ of additional debonding caused by the cyclic loading of each bar).[1] Although any debonding of the bar likely developed gradually throughout the loading history,

Table 3. Energy-dissipating bar properties under monotonic tension loading

Energy-dissipating bar	Sample	Yield strength f_{sy}, ksi	Yield strain ε_{sy},* %	Modulus of elasticity E_s, ksi	Ultimate (peak) strength f_{uel},† ksi	Uniform elongation strain (at f_{uel}) ε_{uel}, %	Strain at bar fracture $\varepsilon_{s,fr}$,‡ %
No. 7: heat 3, specimens 13 and 14	1	69.6	0.23	24,754	95.1	11.30	16.80
	2	69.2	0.25	27,603	94.7	11.42	18.40
	3	69.5	0.26	28,854	94.9	12.13	19.54
	Average	69.4	0.25	27,070	94.9	11.62	18.25
No. 9: heat 2, specimen 15	1	68.3	0.30	27,768	97.8	11.73	17.00
	2	68.3	0.28	27,271	97.5	10.79	14.78
	3	68.1	0.29	26,663	97.5	11.27	14.40
	Average	68.2	0.29	27,234	97.6	11.26	15.39
No. 11: heat 2, specimens 16 to 20	1	65.5	0.24	27,820	93.1	12.91	19.61
	2	65.4	0.25	27,554	92.9	12.42	18.90
	3	65.4	0.23	28,333	92.8	11.86	17.88
	Average	65.4	0.24	27,902	92.9	12.40	18.80

Note: No. 7 = 22M; no. 9 = 29M; no. 11 = 36M; 1 ksi = 6.895 MPa.

* Figure 4 indicates yield point with o markers.

† Figure 4 indicates ultimate strength with ⊿ markers.

‡ Figure 4 indicates bar fracture with ∇ markers.

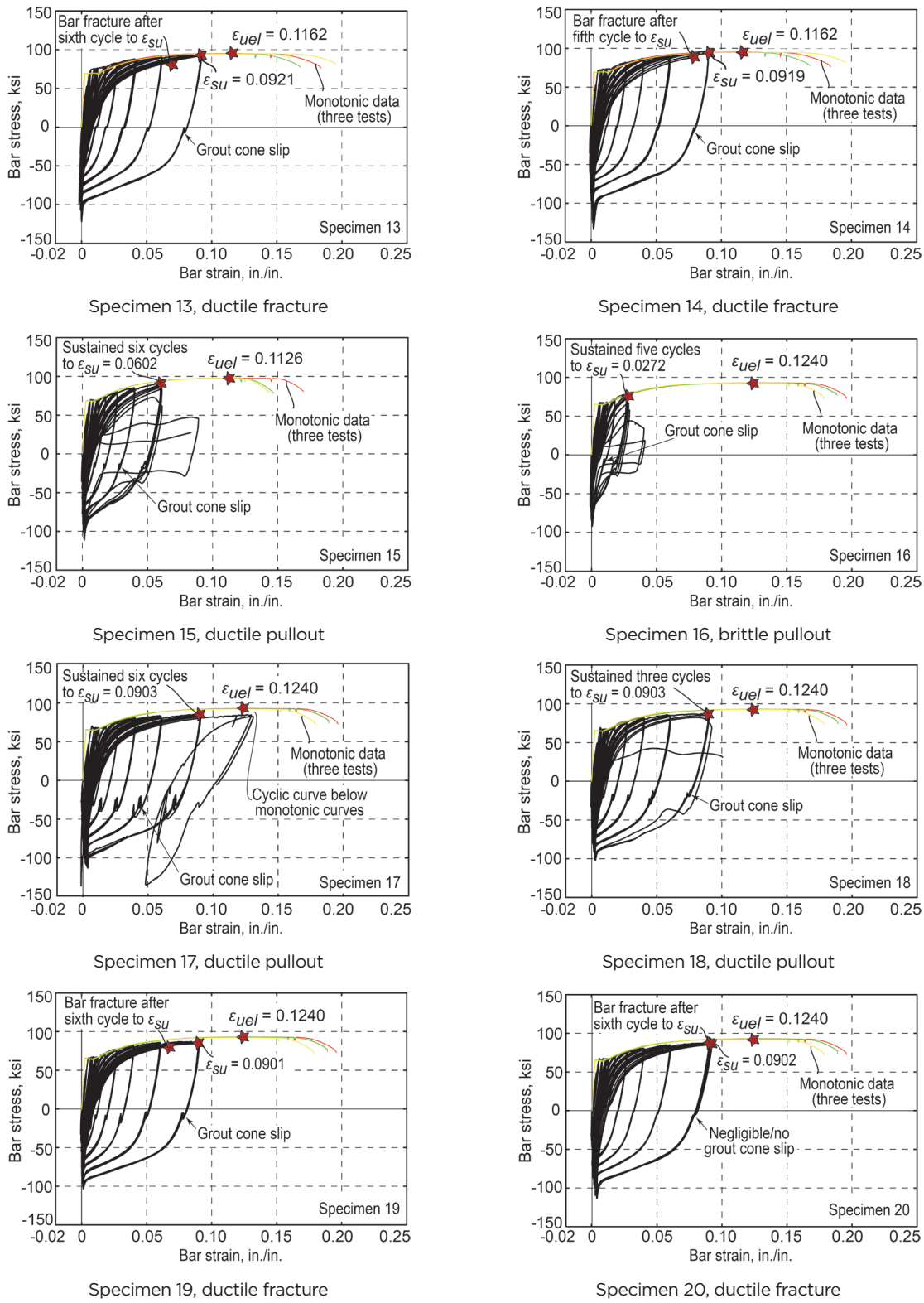

Figure 5. Energy-dissipating bar connection test results. Note: ε_{su} = tension strain amplitude (that is, maximum tension strain) of last loading series (that is, last loading increment) before connection failure under cyclic loading; ε_{uel} = uniform elongation strain of energy-dissipating bar at f_{uel} under monotonic tension loading; f_{uel} = ultimate (maximum) strength of energy-dissipating bar under monotonic tension loading. Monotonic loading results correspond to material tests of isolated bars. 1 in. = 25.4 mm; 1 ksi = 6.895 MPa.

this adjustment term of $1d_b$ was applied to the entire strain history from the LVDTs because it resulted in smaller, and therefore conservative, estimates of the tension strains. Note that there were also two strain gauges located on the wrapped region of each energy-dissipating bar to directly measure the bar strains, but these gauges failed relatively early during each test, which is why the average LVDT displacements were used to approximately estimate the energy-dissipating bar strains.[1] Four different deformation modes—bar straining, bar slip (with respect to the grout), grout deformation (straining), and grout slip (with respect to the connection sleeve)—contributed to the measured total LVDT displacements, but these deformation modes could not be measured separately. Through a numerical study described in Aragon,[10] the bar straining component was determined to be by far the largest component and to contribute approximately 85% to 90% of the measured total LVDT displacements prior to the initiation of connection failure.

Table 4 summarizes the results from the cyclic connection tests in a format similar to those from the previous tests described in Aragon et al.[1,2] These results include the total number of loading cycles sustained (see Aragon et al.[1,2] for

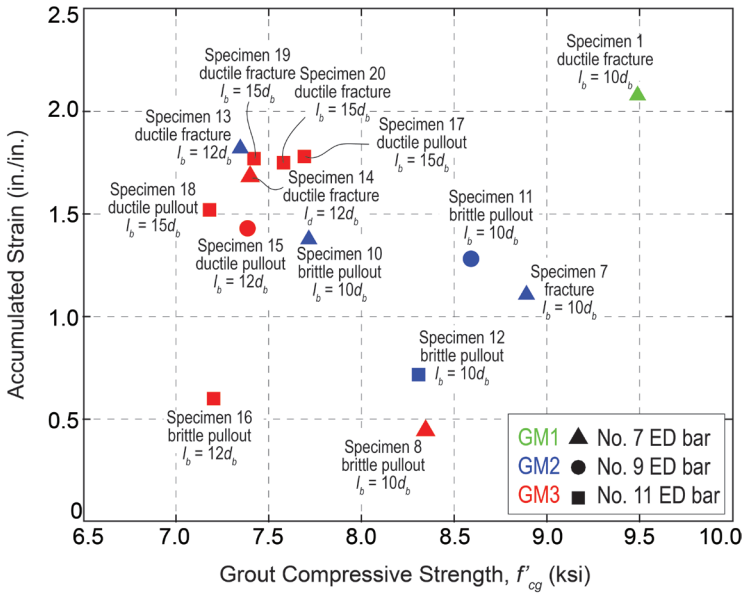

Figure 6. Accumulated strain versus grout compressive strength f'_{cg} for specimens 1, 7, 8, and 10 to 20. Note: d_b = nominal diameter of energy-dissipating bar; l_b = embedment (bond) length of energy-dissipating bar; ED = energy-dissipating. No. 7 = 22M; no. 9 = 29M; no. 11 = 36M; 1 in. = 25.4 mm; 1 ksi = 6.895 MPa.

Table 4. Energy-dissipating bar connection test results

Specimen	Total number of sustained cycles	Accumulated strain, in./in.	Strain amplitude of last loading series ε_{su}	Number of sustained cycles in last loading series	Failure mode
13	74	1.82	0.0921 (0.79ε_{uel})	6	Ductile fracture
14	73	1.69	0.0919 (0.79ε_{uel})	5	Ductile fracture
15	68	1.43	0.0602 (0.53ε_{uel})	6	Ductile pullout
16	55	0.60	0.0272 (0.22ε_{uel})	5	Brittle pullout
17	74	1.78	0.0903 (0.73ε_{uel})	6	Ductile pullout
18	71	1.52	0.0903 (0.73ε_{uel})	3	Ductile pullout
19	74	1.77	0.0901 (0.73ε_{uel})	6	Ductile fracture
20	74	1.75	0.0902 (0.73ε_{uel})	6	Ductile fracture

Note: f_{uel} = ultimate (maximum) strength of energy-dissipating bar under monotonic tension loading; ε_{uel} = uniform elongation strain of energy-dissipating bar at f_{uel} under monotonic tension loading. 1 in. = 25.4 mm.

loading history), accumulated strain, tension strain amplitude of last loading series (that is, last loading increment) ε_{su}, number of cycles sustained in the last loading series, and failure mode. Failure was deemed to have occurred during any cycle with a tension stress drop of 20% or greater from the largest tension stress reached in the entire loading history. The number of sustained cycles in Table 4 is the number of full cycles before this definition of failure. The accumulated strain represents the total amount of tension and compression strain (in absolute value) that each bar was subjected to during all of the sustained cycles. **Figure 6** plots the accumulated strain versus the corresponding grout compressive strength f'_{cg} for specimens 13 to 20, along with specimens 1, 7, 8, and 10 using no. 7 (22M) energy-dissipating bars, specimen 11 using a no. 9 (29M) bar, and specimen 12 using a no. 11 (36M) bar from Aragon et al.,[1,2] for comparison purposes.

Any specimen that sustained six full cycles at a peak tension strain of 0.06 in./in. (0.06 mm/mm) or greater was deemed to have undergone ductile failure (either by low-cycle fatigue fracture or bond pullout of the energy-dissipating bar). As described in Aragon,[10] the requirement to subject the connection to six cycles at each strain increment assumes that the energy-dissipating bars can be placed near the midlength of a precast concrete element, such as a wall, and thus, the bars could undergo tension strain excursions in each of the positive and negative directions of a single lateral wall displacement cycle. Because the experimental validation requirements in ACI ITG-5.1[9] specify a wall specimen to be subjected to three displacement cycles at each loading increment, the energy-dissipating bars placed near the wall midlength would be subjected to six tension strain excursions during each loading increment.

Effect of bond length factor: Objective 1

Specimens 13 and 14 used grout products GM2 and GM3, respectively, with excess water in the grout (that is, reduced compressive strength f'_{cg}) and energy-dissipating bar offset, but with an increased bond length l_b of $12d_b$ (compared with $10d_b$ used in Aragon et al.[1,2]). These specimens specifically investigated the effect of the increased bond length compared with the performance of previously tested specimen 8, which used GM3 with a shorter bond length of $10d_b$ but with no adverse construction conditions.[2] Specimens 13 and 14 both failed by low-cycle fatigue fracture of the energy-dissipating bar and achieved the target strain capacity of 0.06 in./in. (0.06 mm/mm), while specimen 8 did not achieve ductile failure and experienced brittle pullout. Figure 6 shows that specimens 13 and 14 failed at accumulated strains of 1.82 and 1.69 in./in. (1.82 and 1.69 mm/mm), with ε_{su} equal to 0.0921 and 0.0919 in./in. (0.0921 and 0.0919 mm/mm), which correspond to $0.79\varepsilon_{uel}$ and $0.79\varepsilon_{uel}$, respectively. The specimens showed no significant difference in performance between grouts GM2 and GM3 when using a bond length of $12d_b$ and much better performance compared with specimen 8 with GM3 and l_b equal to $10d_b$, which failed at a very low accumulated strain of 0.46 in./in. (0.46 mm/mm). Importantly, the test-day compressive strengths of the grouts in specimens 13 and 14 were very similar ($f'_{cg} \approx 7400$ psi [51.0 MPa]) (Table 2) and considerably lower than the grout strength of $f'_{cg} \approx 8300$ psi (57.2 MPa) in specimen 8. These results demonstrate that by increasing the bond length from $10d_b$ to $12d_b$ (a 20% increase), ductile failure of no. 7 (22M) energy-dissipating bars can be achieved even under adverse conditions and with a grout product (GM3) that had performed especially poorly in a previous test with l_b equal to $10d_b$ (specimen 8).

Effect of energy-dissipating bar size: Objective 2

Failure in specimen 15 (no. 9 [29M] energy-dissipating bar using GM3 with $f'_{cg} \approx 7400$ psi [51.0 MPa]) and specimen 16 (no. 11 [36M] energy-dissipating bar using GM3 with $f'_{cg} \approx 7200$ psi [49.6 MPa]), both with a bond length l_b of $12d_b$, occurred due to progressive debonding and pullout of the bar from the grout, rather than the low-cycle fatigue fracture of the no. 7 (22M) energy-dissipating bars in specimens 13 and 14. The initiation of pullout in specimen 15 was observed after the first full cycle to a strain ε_{su} equal to 0.0602 in./in. (0.0602 mm/mm) (approximately $0.53\varepsilon_{uel}$), with complete pullout (that is, bond failure and stress drop by more than 20%) occurring after the completion of six cycles at this strain level. The bond failure occurred in a ductile manner, achieving six cycles at the target energy-dissipating bar strain of 0.06 in./in. (0.06 mm/mm), but only marginally. Importantly, the accumulated energy-dissipating bar strain–versus–grout compressive strength plot (Fig. 6) shows that the no. 9 energy-dissipating bar in specimen 15, with the increased bond length factor of 12 but a lower grout strength (using GM3 with excess water), achieved an accumulated strain slightly larger than that for the no. 9 bar previously tested in specimen 11 (using GM2 without excess water).[2] These results show that for a no. 9 energy-dissipating bar, despite the adverse conditions incorporated into the connection, it was possible to develop large tension stresses and strains using a slightly increased bond length (l_b equal to $12d_b$ rather than $10d_b$).

Compared with specimen 15, the initiation of pullout in specimen 16 occurred much earlier, after the first full cycle to a strain ε_{su} equal to 0.0272 in./in. (0.0272 mm/mm) (approximately $0.22\varepsilon_{uel}$), with complete pullout after five cycles at this strain level. The grout compressive strength f'_{cg} in specimen 16 was similar to the grout compressive strength of the other specimens in this series of tests. This indicates that connections using greater than a no. 9 (29M) bar ($d_b = 1.128$ in. [28.7 mm]) require a bond length greater than $12d_b$ to achieve the target ductile performance.

Further exploring this finding, **Fig. 7** shows the accumulated strain versus the energy-dissipating bar diameter for specimen 7 (no. 7 [22M] bar), specimen 11 (no. 9 [29M] bar), and specimen 12 (no. 11 [36M] bar) to evaluate the influence of the energy-dissipating bar diameter on the connection ductility. These three specimens were all constructed with a bond length l_b of $10d_b$, a connection sleeve taper angle θ_d of

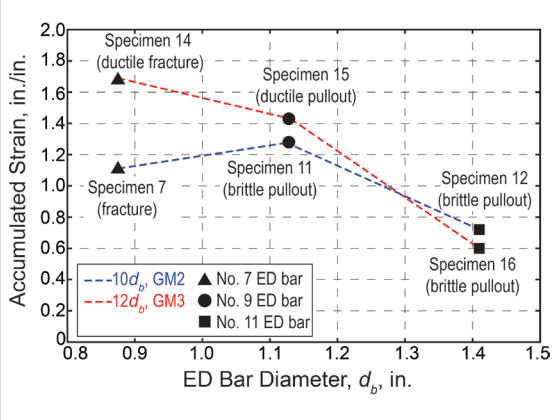

Figure 7. Accumulated strain versus energy-dissipating bar diameter d_b for specimens with 4.5 degree connector sleeve taper angle. Note: ED = energy-dissipating; GM = grout product. No. 7 = 22M; no. 9 = 29M; no. 11 = 36M; 1 in. = 25.4 mm.

4.5 degrees, and grout GM2, and did not include the adverse conditions of excess water in the grout or energy-dissipating bar offset. Figure 7 also shows the results from specimen 14 (no. 7 energy-dissipating bar), specimen 15 (no. 9 bar), and specimen 16 (no. 11 bar). These three specimens were constructed with a bond length of $12d_b$, a connection sleeve taper angle θ_d of 4.5 degrees, and grout GM3, and were tested under the adverse conditions of excess water in the grout and energy-dissipating bar offset. A steep decrease in the accumulated strain capacity occurs with increased energy-dissipating bar diameter, supporting the conclusion that larger-sized bars result in more demanding conditions on the connector despite the proportionally increased bond length. The one exception to this trend is specimen 7; however, the strain capacity of this specimen was limited by premature low-cycle fatigue fracture of the energy-dissipating bar, which prevented the connection from being tested under greater stresses and strains.

Based on the results in Fig. 7, it is recommended that the bond length factor be increased with increasing bar size. Under the adverse conditions tested, a bond length factor of 12 was found to be adequate to achieve ductile fracture of no. 7 (22M) energy-dissipating bars (specimens 13 and 14) and ductile bond failure (pullout) of no. 9 (29M) energy-dissipating bars (specimen 15). However, under similar adverse conditions, a larger bond length factor was necessary to achieve ductile failure of no. 11 (36M) bars. As such, the bond length of the no. 11 energy-dissipating bars in specimens 17 to 20 was increased from $12d_b$ to $15d_b$ (l_b = 21.15 in. [537 mm]). Specifically looking at specimen 19, which had θ_d = 4.5 degrees and $f'_{cg} \approx$ 7400 psi [51.0 MPa], similar to specimen 16 but with a longer l_b of $15d_b$, the connection achieved ductile failure through low-cycle fatigue fracture of the energy-dissipating bar after six cycles at strain ε_{su} equal to 0.0901 in./in. (0.0901 mm/mm), or approximately $0.73\varepsilon_{uel}$. Expanding on this finding, **Fig. 8** shows the accumulated strain versus bond length factor for specimens that had a connection sleeve taper angle θ_d of 4.5 degrees and used grout product GM3: specimens 8 and 14, which used no. 7 energy-dissipating bars with bond length factors of 10 and 12, respectively, and specimens 16 and 19, which used no. 11 energy-dissipating bars with bond length factors of 12 and 15, respectively. Unlike specimen 8, specimens 14, 16, and 19 were tested with the adverse conditions of excess water in the grout and energy-dissipating bar offset. The results show significant increases in the accumulated strain capacity as the bond length factor increases, even under adverse conditions, and demonstrate that the increased bond length of $15d_b$ can result in satisfactory connection performance for no. 11 energy-dissipating bars. Further tests are needed to determine the appropriate bond length factors for bar diameters not investigated in this

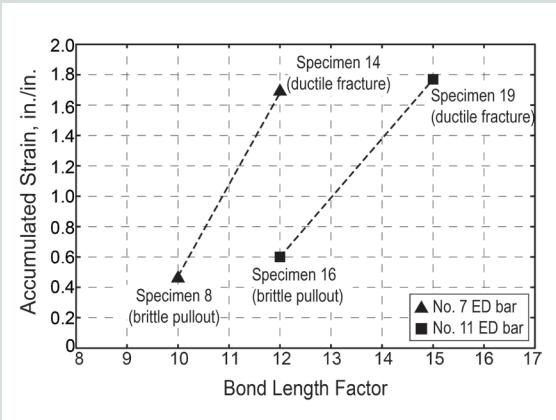

Figure 8. Accumulated strain versus energy-dissipating bar bond length factor for specimens with 4.5-degree connector sleeve taper angle and grout product GM3. Note: ED = energy-dissipating; GM = grout product. No. 7 = 22M; no. 11 = 36M; 1 in. = 25.4 mm.

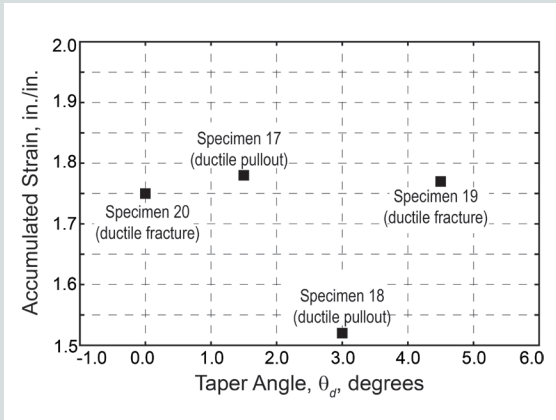

Figure 9. Accumulated strain versus connector sleeve taper angle θ_d for no. 11 energy-dissipating bars with l_b equal to $15d_b$ embedded in grout product GM3. Note: d_b = nominal diameter of energy-dissipating bar; GM = grout product; l_b = embedment (bond) length of energy-dissipating bar. No. 11 = 36M; 1 in. = 25.4 mm.

experimental program and under different loading scenarios, such as combined axial and lateral loading. Also, because the required bond length to achieve ductile connection behavior is not proportional to the bar diameter, other forms for the relationship between the bar bond length and bar diameter should be investigated.

Effect of sleeve taper angle: Objective 3

Specimens 17 to 20 with increased l_b of $15d_b$ (21.15 in. [537 mm]) specifically focused on the effect of the sleeve taper angle θ_d on the connection performance. **Figure 9** shows the accumulated strain versus the connector taper angle for specimen 17 (θ_d = 1.5 degrees, without corrugations, and $f'_{cg} \approx$ 7700 psi [53.1 MPa]), specimen 18 (θ_d = 3.0 degrees, without corrugations, and $f'_{cg} \approx$ 7200 psi [49.6 MPa]), specimen 19 (θ_d = 4.5 degrees, without corrugations, and $f'_{cg} \approx$ 7400 psi [51.0 MPa]), and specimen 20 (θ_d = 0.0 degrees, with corrugations, and $f'_{cg} \approx$ 7600 psi [52.4 MPa]). These four specimens all used no. 11 (36M) energy-dissipating bars and grout product GM3 under the adverse conditions of excess water in the grout and energy-dissipating bar offset, and all achieved almost identical maximum strain amplitudes of $\varepsilon_{su} \approx$ 0.09 in./in. (0.09 mm/mm) (Fig. 5) or approximately $0.73\varepsilon_{uel}$. However, the accumulated strain for specimen 18 was somewhat lower because it sustained only three cycles at ε_{su}, whereas specimens 17, 19, and 20 sustained six cycles at ε_{su}. The failure mechanisms for the specimens also differed. Specimen 17 (θ_d = 1.5 degrees) failed by progressive pullout of the grout cone from the connection sleeve, specimen 18 (θ_d = 3.0 degrees) failed by progressive pullout of the energy-dissipating bar from the grout, and specimens 19 (θ_d = 4.5 degrees) and 20 (θ_d = 0.0 degrees with corrugations) failed by energy-dissipating bar fracture. These results suggest that a connector with taper angle of 3.0 degrees and no corrugations was not as effective as a straight sleeve with corrugations or a smooth 4.5-degree tapered sleeve, yet it provided enough confinement to prevent excessive slip of the grout cone, as was observed with the 1.5-degree tapered sleeve.

Although all three specimens 17 to 19 with connection sleeve taper angles θ_d equal to 1.5, 3.0, and 4.5 degrees, respectively, failed at similar accumulated strains and after almost identical maximum strains ε_{su} (Table 4), important observations were made regarding the effect of the sleeve taper angle and other factors on the connection behavior. Similar to the behavior of the previous specimens in Aragon et al.,[1,2] progressive upward slip of the grout cone with respect to the connection sleeve was observed as each energy-dissipating bar was loaded in tension. Upon load reversal into compression, an instantaneous reversal of this slip (and accompanying loud noise from the released energy) occurred in all of the specimens with a tapered sleeve. The energy-dissipating bar stress-strain plots in Fig. 5 show the sudden small reduction in strain as the response cycle crosses from tension into compression loading. The large energy release from the sudden reversal of grout cone slip may have caused greater (impact) stresses in the grout. The progressive upward slip of the grout cone was visible during the later loading series when the gap between the wall-panel and foundation blocks was large enough. The noise associated with slip reversal began to subside toward the end of the tests that had failure through bar pullout. Importantly, increased bond length from $12d_b$ to $15d_b$ (specimens 16 and 19) and the associated increase in connector sleeve length did not result in a reduction in grout cone slip, indicating that corrugations are needed on the connection sleeve to reduce grout cone slip.

Except for specimen 20 with a straight but corrugated sleeve, the contribution of grout cone slip to the total tensile deformation of the connection increased as the taper angle θ_d decreased because there were no surface corrugations on the tapered sleeves to prevent sliding of the grout cone. Specimen 17 with θ_d of 1.5 degrees had the largest amount of grout cone slip. The measured stress-strain behavior of specimen 17 (Fig. 5) also exhibited the largest sudden strain reduction associated with grout cone slip (and the loudest accompanying noise) upon load reversal into compression compared with specimens 18 and 19 with larger sleeve taper angles. As a result of the excessive grout cone slip, the tension stress envelope of the measured cyclic stress-strain behavior for specimen 17 was considerably lower than the monotonic stress-strain behavior from energy-dissipating bar material testing. This means that the actual energy-dissipating bar strains during cyclic connection testing were smaller than the strains shown in Fig. 5, resulting in smaller measured bar stresses. Because the strain gauges on the bar failed relatively early in each test, and without a method to measure slip independently, it was not possible to accurately measure the energy-dissipating bar strains during the large deformations of the cyclic connection tests.[1,2]

As a result of the excessive grout cone slip, specimen 17 did not experience a stress drop exceeding the 20% threshold used to define ultimate failure in the other specimens, which resulted in this specimen, with θ_d of 1.5 degrees, being the most ductile in the entire experimental program. Nonetheless, the specimen was deemed to have failed after sustaining six cycles at ε_{su} equal to 0.0903 in./in. (0.0903 mm/mm). During the last cycle of loading beyond ε_{su}, the gap-opening displacement between the wall-panel and foundation blocks extended beyond the thickness of the guiding column base plates (Fig. 1), which were used to prevent rotations of the wall panel. Upon reversal of loading, the wall-panel block rotated slightly because it was no longer restrained by the column base plates and came in contact with the top of the column base plate on one side. This prevented testing from continuing to full failure (that is, reaching a stress drop of greater than 20%).

A corrugated sleeve with θ_d equal to 1.5 degrees may have improved the behavior of the connection by reducing the amount of grout cone slip, but this configuration was not tested. Specimen 18 with θ_d of 3.0 degrees failed through ductile pullout of the energy-dissipating bar from the connection grout. These results suggest that the 3.0-degree tapered

smooth sleeve was not as effective as the straight sleeve with corrugations (specimen 20) or the 4.5-degree tapered smooth sleeve (specimen 19), yet it provided enough confinement to prevent the excessive slip of the grout cone observed in specimen 17 with the 1.5-degree tapered smooth sleeve. The corrugations and dimples[10] on the surface of the straight sleeve (Fig. 2) were of vital importance because they prevented the grout from slipping with respect to the sleeve. No loud noise was heard during the testing of specimen 20, and there was no sudden strain reduction upon load reversal into compression on the measured stress-strain behavior (indicating no impact load on the connection), supporting the conclusion that there was no significant slip of the grout inside the straight corrugated sleeve.

The excellent performance of specimen 20 with the straight corrugated sleeve (achieving energy-dissipating bar fracture after the completion of six cycles to ε_{su} of 0.0902 in./in. [0.0902 mm/mm]) shows that with a bond length factor of 15 and adequate sleeve corrugations, a straight sleeve can develop large tension stresses and strains in energy-dissipating bars as large as no. 11 (36M), even with a bar offset and excess water in the grout. This is a substantial finding that can significantly reduce the cost of the connection because various sizes of commercially available corrugated steel pipe used in the post-tensioning industry are readily available from multiple manufacturers. In addition, straight sleeves would minimize the required distance between adjacent energy-dissipating bars in a full-scale structure compared with bars in tapered sleeves.

Effect of connection grout product

An important goal in developing this nonproprietary ductile connection was for it not to require a specific grout product. Therefore, three different grout products (GM1, GM2, and GM3) were investigated in the research program.[1,2] These materials were chosen because they are high-performance grouts and are commercially available in the United States. In general, connections with grout products GM1 and GM2 performed considerably better under cyclic loading than connections using grout product GM3.[2] Specimens 13 to 20 all used the lowest-performing grout product from previous tests, GM3, while also incorporating adverse conditions from possible construction errors and inaccuracies. Figure 6 shows the accumulated strain versus grout compressive strength f'_{cg} for specimens 1, 7, 8, 10, 13, and 14, which all used no. 7 (22M) energy-dissipating bars and a connector sleeve taper angle θ_d of 4.5 degrees with a bond length factor of 10 or 12. The grout products in specimens 1, 7, and 8 were mixed according to each manufacturer's specifications and reached compressive strengths greater than 8000 psi (55.2 MPa). Specimen 10 included excess water in the grout during mixing but no energy-dissipating bar offset, while specimens 13 and 14 included excess water in the grout and energy-dissipating bar offset. The results show that under these adverse conditions and with an increased bond length of $12d_b$ for no. 7 energy-dissipating bars, both grout products GM2 and GM3 (specimens 13 and 14, respectively) successfully achieved the desired behavior of the connection.

For larger energy-dissipating bar sizes, consider specimens 15 to 20 and specimens 11 and 12 (Fig. 6). Specimen 15 (no. 9 [29M] energy-dissipating bar) and specimens 16 to 20 (no. 11 [36M] bars) all used the lowest-performing grout product, GM3, under adverse conditions, while specimens 11 and 12 (no. 9 and 11 bars, respectively) used grout product GM2 without any adverse conditions. The results show that the no. 9 bar in specimen 15, with the increased bond length factor of 12 but lower grout strength, achieved an accumulated strain capacity slightly larger than that of the no. 9 bar in specimen 11. Similarly, all of the no. 11 bars with a bond length factor of 15 (specimens 17 to 20) constructed under adverse conditions achieved much higher accumulated strains compared with those with a bond length factor of 10 or 12 (specimens 12 and 16, respectively). These results show that for no. 9 and 11 energy-dissipating bars, despite the adverse conditions incorporated into the connection, it was possible to develop large cyclic stresses and strains using bond length factors of 12 and 15, respectively.

Performance of wall-panel and foundation blocks

The 28-day compressive strengths of the wall-panel and foundation block concrete $f'_{c,28d}$ were approximately 4100 and 4750 psi (28.3 and 32.8 MPa) for specimens 13 and 14 and 15 to 20, respectively. Similar to the previous experiments, no damage was visible on the wall-panel concrete for any of the test specimens.[1,2] In the foundation block, short hairline cracks were observed extending outward from the edge of the connector sleeve at the top (similar to the foundation block cracking shown in Aragon et al.[2]). The largest measured tie reinforcement strains in the foundation block of specimens 13 and 14 (with no. 7 [22M] energy-dissipating bars) were 0.001624 in./in. (0.001624 mm/mm) and 0.00102 in./in. (0.00102 mm/mm) for the vertical and horizontal tie bars, respectively. For specimen 15, which used a no. 9 (29M) energy-dissipating bar, the largest measured reinforcement strains were 0.001248 in./in. (0.001248 mm/mm) and 0.000928 in./in. (0.000928 mm/mm) in the vertical and horizontal tie bars, respectively. For specimens 16 to 20 with no. 11 (36M) energy-dissipating bars, the largest measured strains were 0.001653 in./in. (0.001653 mm/mm) and 0.001056 in./in. (0.001056 mm/mm) in the vertical and horizontal tie bars, respectively. All of the strains measured in the tie reinforcement were smaller than the yield strain of the bars. These results support that the strut-and-tie design methodology used for the tie reinforcement described in Aragon et al.[1] was appropriate and conservative.

In all of the 20 tests conducted as part of this research program, the vertical tie bar strains were larger and closer to the yield strain than the horizontal tie bar strains. This indicates that the horizontal tie reinforcement areas could have been decreased. However, connections under more realistic conditions (such as energy-dissipating bar groups under combined axial and lateral

loading) could result in more demanding conditions for the tie reinforcement. As such, the apparent additional capacity provided by the horizontal tie reinforcement from the strut-and-tie model is deemed desirable for design purposes.

Conclusion

This paper extends previous experimental results (involving 12 specimens) of a ductile cementitious-grouted connection for energy-dissipating deformed steel reinforcing bars at gap-opening base joints in seismic precast concrete structures.[1,2] Eight additional connection tests and accompanying energy-dissipating bar, grout, and concrete material tests were conducted varying the following parameters: grout product, energy-dissipating bar bond (embedment) length l_b, energy-dissipating bar diameter d_b, and connector sleeve taper angle θ_d and corrugations. The tests also incorporated adverse conditions from increased water in the grout and energy-dissipating bar axial offset within the connector sleeve. The main conclusions from these tests are as follows:

- Larger-diameter energy-dissipating bars resulted in more demanding conditions on the connector grout, despite the proportionally increased bond length when using a constant bond length factor (for example, $l_b = 10d_b$ with a bond length factor of 10). Therefore, for ductile behavior, the bond length factor should be increased for larger bar diameters.

- A bond length factor of 12 was found to be adequate for achieving ductile low-cycle fatigue fracture for no. 7 (22M) energy-dissipating bars and ductile bond failure (that is, ductile pullout of the energy-dissipating bar) for no. 9 (29M) bars. A greater bond length factor of 15 was necessary to achieve ductile failure (through energy-dissipating bar fracture) of no. 11 (36M) bars.

- The desired ductile behavior using these bond length factors was achieved under the adverse construction conditions considered in this paper and with the lowest-performing grout product (GM3) investigated in the research program. This is an important finding and allows the use of the connection without requiring a specific grout product or excessively tight field application tolerances.

- Further tests are needed to determine the appropriate bond length factors for bar diameters not investigated in this experimental program and under different loading scenarios, such as combined axial and lateral loading. Also, because the required bond length to achieve ductile connection behavior is not proportional to the bar diameter, other forms for the relationship between the bar bond length and bar diameter should be investigated.

- A smooth connector sleeve with a taper angle θ_d of 1.5 degrees was the most ductile of all specimens tested in this experimental program. Specifically, there was no significant stress drop in the energy-dissipating bar during the test, and therefore failure of the connection was not fully reached. This behavior occurred through progressive but incomplete pullout of the grout cone with respect to the connector sleeve. A sleeve with corrugations, still with θ_d equal to 1.5 degrees, may improve the behavior of the connection; however, this configuration was not tested in the experimental program.

- Although energy-dissipating bars in tapered connection sleeves achieved ductile failure, as well as being the most ductile connection when using θ_d of 1.5 degrees, a taper is not necessary as long as a straight steel sleeve with adequate corrugations is used with a bond length factor of 12 for no. 7 and 9 (22M and 29M) energy-dissipating bars and 15 for no. 11 (36M) bars. As such, corrugated straight steel pipe is the recommended connection sleeve resulting from this research. This is a substantial finding that can significantly reduce the cost of the connection because various sizes of steel pipe used in the post-tensioning industry are readily available from multiple manufacturers. Importantly, straight sleeves minimize the required distance between adjacent energy-dissipating bars compared with tapered sleeves, which have a larger bottom diameter than the entrance (top) diameter. Unlike tapered sleeves, corrugations are necessary on straight connection sleeves because straight sleeves do not provide the wedging effect to the grout that tapered sleeves provide.

- In the smooth tapered sleeve connections, upward slip of the grout cone with respect to the sleeve surface was observed as the energy-dissipating bar was loaded in tension. Upon load reversal into compression, sudden reversal of this slip (and accompanying loud noise and impact from the released energy) occurred in all of the specimens with a tapered sleeve. An increase in the taper angle tended to decrease the slip of the grout cone under tension loading of the energy-dissipating bar, resulting in decreased slip reversal upon loading back into compression. The straight corrugated sleeves had less grout cone slip and thus less impact load on the connection.

- Small (hairline) concrete cracking and linear-elastic tie reinforcement strains in the foundation validated the strut-and-tie design of the tie reinforcement around the connection for energy-dissipating bars of varying diameters.

Note that although the test variables in this experimental program were selected to determine trends, some of the findings may be limited to the specimens and materials tested. Because of the cost and time required to conduct each energy-dissipating bar connection experiment, there were no identical connection specimens tested to demonstrate the repeatability of the results. In addition, the applied uniaxial loading condition on the connections was not fully representative of the combined axial and lateral loading on an energy-dissipating bar in a rocking wall, pier, or column subjected to earthquake loading.

Acknowledgments

This paper is based on work supported by a PCI Daniel P. Jenny Research Fellowship and a National Science Foundation Graduate Research Fellowship under grant DGE-1144468. The authors acknowledge the support of the PCI Research and Development Council, the PCI Central Region, and members of its Industry Advisory Committee, including Ned Cleland of Blue Ridge Design, Tom D'Arcy of Consulting Engineers Group, David Dieter of Mid-State Precast, Sameh El Ashri of e.construct Dubai, S. K. Ghosh of S. K. Ghosh Associates, Harry Gleich of Metromont Corp., Neil Hawkins of University of Illinois–Urbana-Champaign, and Larbi Sennour of Consulting Engineers Group. In addition, the authors gratefully acknowledge the support of StresCore Inc. and Dayton Superior Corp. for providing material donations and assistance to the project. Any opinions, findings, conclusions, and recommendations expressed in the paper are those of the authors and do not necessarily reflect the views of the individuals and organizations acknowledged.

References

1. Aragon, T. A., Y. C. Kurama, and D. F. Meinheit. 2017. "A Type III Grouted Seismic Connector for Precast Concrete Structures." *PCI Journal* 62 (5): 75–88.

2. Aragon, T. A., Y. C. Kurama, and D. F. Meinheit. 2019. "Effects of Grout and Energy Dissipating Bar Properties on a Type III Grouted Seismic Connection for Precast Structures." *PCI Journal* 64 (1): 31–48.

3. ASTM Subcommittee A01.05. 2016. *Standard Specification for Deformed and Plain Low-Alloy Steel Bars for Concrete Reinforcement*. ASTM A706/A706M. West Conshohocken, PA: ASTM International.

4. ACI (American Concrete Institute) Innovation Task Group 5. 2009. *Requirements for Design of a Special Unbonded Post-Tensioned Precast Shear Wall Satisfying ACI ITG-5.1 and Commentary*. ACI ITG-5.2. Farmington Hills, MI: ACI.

5. Smith, B. J., Y. C. Kurama, and M. J. McGinnis. 2012. "Hybrid Precast Wall Systems for Seismic Regions." Structural engineering research report NDSE-2012-01. Department of Civil and Environmental Engineering and Earth Sciences, University of Notre Dame, Notre Dame, IN. https://www3.nd.edu/~ykurama/REPORT_NDSE-12-01.pdf.

6. ACI Committee 318. 2014. *Building Code Requirements for Structural Concrete (ACI 318-14) and Commentary (ACI 318R-14)*. Farmington Hills, MI: ACI.

7. Smith, B. J., and Y. C. Kurama. 2014. "Seismic Design Guidelines for Solid and Perforated Hybrid Precast Concrete Shear Walls." *PCI Journal* 59 (3): 43–49.

8. Smith, B. J., Y. C. Kurama, and M. J. McGinnis. 2015. "Perforated Hybrid Precast Shear Walls for Seismic Regions." *ACI Structural Journal* 112 (3): 359–370.

9. ACI Innovation Task Group 5. 2007. *Acceptance Criteria for Special Unbonded Post-Tensioned Precast Structural Walls Based on Validation Testing and Commentary*. ACI ITG-5.1. Farmington Hills, MI: ACI.

10. Aragon, T. A. 2018. "Type III Grouted Ductile Reinforcing Bar Connections for Precast Concrete Structures." PhD diss., Department of Civil and Environmental Engineering and Earth Sciences, University of Notre Dame, Notre Dame, IN.

11. ASTM Subcommittee A01.05. 2016. *Standard Specification for Deformed and Plain Carbon-Steel Bars for Concrete Reinforcement*. ASTM A615/A615M. West Conshohocken, PA: ASTM International.

12. ASTM Subcommittee C09.43. 2014. *Standard Specification for Packaged Dry, Hydraulic-Cement Grout (Nonshrink)*. ASTM C1107/C1107M. West Conshohocken, PA: ASTM International.

13. ASTM Subcommittee A05.11. 2017. "Standard Specification for Steel Sheet, Zinc-Coated (Galvanized) or Zinc-Iron Alloy-Coated (Galvannealed) by the Hot-Dip Process." ASTM A653/A653M. West Conshohocken, PA: ASTM International.

14. Kurama, Y. C. 2005. "Seismic Design of Partially Post-Tensioned Precast Concrete Walls." *PCI Journal* 50 (4): 100–125.

Notation

d_b = nominal diameter of energy-dissipating bar

d_{corr} = depth of surface corrugations on connector sleeve

E_s = modulus of elasticity of energy-dissipating bar

$f'_{c,28d}$ = compressive strength of foundation and wall-panel block concrete at 28 days

f'_{cg} = compressive strength of grout on day of energy-dissipating bar connection testing

$f'_{cg,28d}$ = compressive strength of grout at 28 days

$f_{s,fr}$ = stress in energy-dissipating bar at bar fracture under monotonic tension loading

f_{sy} = yield strength of energy-dissipating bar

f_{uel} = ultimate (maximum) strength of energy-dissipating bar under monotonic tension loading

h_f = height of foundation block

h_w = height of wall-panel block

l_b = embedment (bond) length of energy-dissipating bar

l_f = length of foundation block

l_{su} = total unbonded length of energy-dissipating bar (wrapped length plus additional debonded length expected under cyclic loading)

l_{sw} = wrapped length of energy-dissipating bar

l_w = length of wall-panel block

t_w = thickness of wall-panel block

w_f = width of foundation block

$\varepsilon_{s,fr}$ = strain in energy-dissipating bar at bar fracture under monotonic tension loading

ε_{su} = tension strain amplitude (that is, maximum tension strain) of last loading series (that is, last loading increment) before energy-dissipating bar connection failure under cyclic loading

ε_{sy} = yield strain of energy-dissipating bar

ε_{uel} = uniform elongation strain of energy-dissipating bar at f_{uel} under monotonic tension loading

θ_d = taper angle of energy-dissipating bar connector sleeve

About the authors

Theresa Aragon, PhD, is a faculty member in the School of Math, Science, and Engineering at Central New Mexico Community College in Albuquerque, N.Mex.

Yahya Kurama, PhD, PE, is a professor in the Department of Civil and Environmental Engineering and Earth Sciences at the University of Notre Dame in Notre Dame, Ind.

Donald Meinheit, PhD, PE, SE, is a principal at Wiss, Janney, Elstner Associates Inc. in Chicago, Ill.

Abstract

This paper describes an experimental investigation of the cyclic uniaxial behavior of a grouted reinforcing bar–to–foundation connection that can develop ductility under seismic loading even when constructed with adverse conditions. The connector comprises a cylindrical thin metal sleeve, with or without a taper, embedded inside the foundation and filled with flowable cementitious grout to anchor an ASTM A706 Grade 60 (414 MPa) steel reinforcing bar over a short embedment (bond) length. The paper extends previous published experiments involving 12 specimens on the performance of this connection under ideal laboratory conditions to eight additional tests conducted under simulated adverse effects from off-center placement of the reinforcing bar inside the connection sleeve and reduced grout strength by using excess water in the grout mixture. The specimens were tested with the objective of reaching close to the full ultimate strength of each reinforcing bar under a rigorous cyclic axial strain loading history. The test parameters included the grout product, bar embedment length, bar diameter, connector sleeve taper angle, and connector sleeve surface corrugations. The results showed that reinforcing bars anchored over a short embedment length of 12 times the bar diameter for no. 7 and 9 bars (22M and 29M) or 15 times the bar diameter for no. 11 bars (36M) can achieve ductile cyclic behavior even under the adverse conditions that were considered.

Keywords

Construction tolerance, deformed reinforcing bar, ductile connection, energy-dissipating steel bar, gap-opening joint, grouted seismic connector, low-cycle fatigue fracture, pull-out (bond) failure, seismic, straight grout sleeve, tapered grout sleeve, Type III connection, uniform elongation strain.

Review policy

This paper was reviewed in accordance with the Precast/Prestressed Concrete Institute's peer-review process.

Reader comments

Please address any reader comments to *PCI Journal* editor-in-chief Tom Klemens at tklemens@pci.org or Precast/Prestressed Concrete Institute, c/o *PCI Journal*, 8770 W. Bryn Mawr Ave., Suite 1150, Chicago, IL 60631.